Available online at www.sciencedirect.com
SCIENCE DIRECT®
Journal of Solid State Chemistry 177 (2004) 3301–3309
JOURNAL OF SOLID STATE CHEMISTRY
http://elsevier.com/locate/jssc

Defect clusters and precipitation/oxidation of MgO–$Co_{1-x}O$ solid solution ☆

T.M. Tsai, K.C. Yang, and P. Shen*

Institute of Materials Science and Engineering, National Sun Yat-sen University, Kaohsiung, 80424 Taiwan, ROC

Received 16 January 2004; received in revised form 19 April 2004; accepted 25 April 2004

Available online 20 July 2004

Abstract

MgO and $Co_{1-x}O$ powders in 9:1 and 1:9 molar ratio (denoted as M_9C_1 and M_1C_9, respectively) were sintered and homogenized at 1600°C followed by annealing at 850°C and 800°C, respectively to form defect clusters and precipitates. Analytical electron microscopic observations indicated the protoxide remained as rock salt structure with complicated planar diffraction contrast for M_9C_1 sample, however with spinel paracrystal precipitated from the M_1C_9 sample due to the assembly of charge- and volume-compensating defects of the 4:1 type, i.e., four octahedral vacant sites surrounding one Co^{3+}-filled tetrahedral interstitial site. The spacing of such defect clusters is 4.5 times the lattice spacing of the average spinel structure of Mg-doped $Co_{3-\delta}O_4$, indicating a higher defect cluster concentration than undoped $Co_{3-\delta}O_4$. The {111} faulting of Mg-doped $Co_{3-\delta}O_4/Co_{1-x}O$ in the annealed M_1C_9 sample implies the possible presence of zinc blend-type defect clusters with cation vacancies assembled along oxygen close packed (111) plane.

Keywords: $Co_{1-x}O$,MgO; Solid solution; Mg-doped $Co_{3-\delta}O_4$ spinel; Defect clusters; Paracrystal; Fault; AEM

1. Introduction

The motivation of this research was to compare the aging behavior of Mg- and Co-rich compositions in the solid solution phase field of MgO–$Co_{1-x}O$ with rock salt structure. Using analytical electron microscopy (AEM), we focused on the precipitation of the spinel paracrystal from the Co-rich end in drastic contrast with planar defect modulation from the Mg-rich end.

The paracrystalline distribution is such that the spacing between defects remains fairly constant but the relative lateral translation may occur more variably [1,2]. $Fe_{1-x}O$ having a considerable degree of nonstoichiometry ($x<0.15$ [3]) was known to possess defect clusters of 4:1 type with four octahedral vacant sites surrounding one Fe^{3+}-filled tetrahedral interstitial site [4]. When aged at high temperatures, the 4:1 clusters may assemble into larger units (e.g. 13:4, 16:5 and form a paracrystal [1,2]), which order further into Fe_3O_4 spinel or other ordered phases: p'' and p''' [5,6].

$Co_{1-x}O$ with a much smaller x (ca. 0.01 [7]) than $Fe_{1-x}O$ also formed spinel-type lattice of $Co_{3-\delta}O_4$, which is surprisingly with paracrystalline distribution of defect clusters while prepared by oxidizing/sintering $Co_{1-x}O$ in air [8]. ($Co_{3-\delta}O_4$ is a normal type spinel according to magnetic measurements [9] and can be formed by spontaneous oxidation of $Co_{1-x}O$ upon cooling below 900°C [10].) By contrast with $Co_{1-x}O$ (band gap 2.7 eV) [11], MgO has a much wider band gap (6.8 eV) [12] and two orders of magnitude lower in the extent of nonstoichiometry. Intrinsic MgO with 100 ppm magnesium vacancies was reported to remain highly ionic rather than electronic up to 1300 K [13]. The research focus on the defects of MgO has been the effect of temperature, stress and impurity on the behavior of dislocations [14].

According to the phase diagram [15], the MgO–$Co_{1-x}O$ system forms complete solid solution at high temperatures in air and decomposes below ca. 850°C into Mg-doped (<1 at%) $Co_{3-\delta}O_4$ spinel and protoxide of a wide Co/(Mg+Co) atomic ratio. From 850°C to

☆ Supplementary data associated with this article can be found, in the online version, at doi=10.1016/j.jssc.2004.04.061

*Corresponding author. Fax: +886-7-5254099.
E-mail address: pshen@mail.nsysu.edu.tw (P. Shen).

0022-4596/$ - see front matter © 2004 Elsevier Inc. All rights reserved.
doi:10.1016/j.jssc.2004.04.061

600°C in air, the protoxide that equilibrates with Mg-doped $Co_{3-\delta}O_4$ spinel was alleged to have the atomic ratio Co/(Mg + Co) decreasing from 99% to ca. 2% [15]. Here we proved experimentally that planar defect modulation and spinel paracrystal occur in the Mg- and Co-rich protoxide, respectively when the MgO–$Co_{1-x}O$ solid solution was fired in this temperature range in air. We showed also that the paracrystal spacing of $Co_{3-\delta}O_4$ spinel was tailored by Mg dopant and {111} specific fault generated in both the rock salt and spinel structures upon annealing of Mg-doped $Co_{1-x}O/Co_{3-\delta}O_4$.

2. Experimental

MgO (Cerac 99.9%, 5 μm) and $Co_{1-x}O$ (Cerac 99.9%, 2 μm) powders in 9:1 and 1:9 molar ratio (denoted as M_9C_1 and M_1C_9, respectively) were ball milled in alcohol, oven dried at 100°C, and then dry pressed at 650 MPa to form pellets ca. 5 mm in diameter and 2 mm in thickness. The pellets of M_1C_9 and M_9C_1 were sintered and homogenized at 1600°C for 5 h and then quenched in air. The sintered M_1C_9 and M_9C_1 specimens were further aged at 800°C for 72 h and 850°C for 96 h, respectively, followed by the quenching in air. (A slightly higher annealing temperature and dwelling time was employed for the more refractory M_9C_1 sample.)

X-ray diffraction (XRD, Cu$K\alpha$, 40 kV, 30 mA, at 0.05° and 3 s per step from 2θ angle of 15° up to 120°) was used to identify the phases of the fired specimens. Scanning electron microscopy (SEM, JSM-6400, 20 kV) was used to study thermally etched (1500°C for 10 min) surface for the distribution of grains and pores in the fired specimen. Thin sections of the samples were Ar-ion milled to electron transparency and studied by AEM (JEOL 3010) at 300 kV for bright field image, dark field image, lattice image, selected area electron diffraction (SAED) pattern, and point-count energy dispersive X-ray (EDX) analysis. The EDX analysis was performed using K shell counts for Mg, Co and O, and the principle of ratio method without absorption correction [16]. The error was estimated to be within ±5%.

3. Results

3.1. XRD and SEM

XRD indicated the M_9C_1 samples fired at 1600°C for 5 h (Fig. 1a) or subject to further annealing at 850°C for 96 h (Fig. 1b) contain only protoxide of rock salt structure. Least-squares fit of the d-spacings indicated the protoxide has a lattice parameter of 0.4223 and 0.4228 ± 0.0001 nm, respectively for the samples fired at

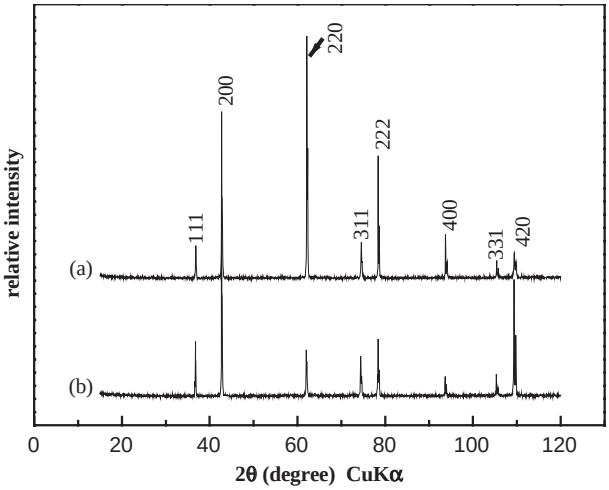

Fig. 1. XRD traces for the protoxide of rock salt structure in M_9C_1 sample: (a) fired at 1600°C for 5 h and (b) subject to further annealing at 850°C for 96 h and then air-quenched.

1600°C and 850°C. These lattice parameters are considerably larger than undoped MgO (0.4211 nm, JCPDS#45-0946) and smaller than undoped $Co_{1-x}O$ (0.4260 nm, JCPDS#09-0402) indicating a considerable dissolution of larger-size Co^{2+} in MgO. The temperature dependence of lattice parameter may be due to spin state change of Co^{2+} in coordination number (CN) 6 [17] as discussed later. Assuming a linear composition dependence of lattice parameters, the protoxide formed at 850°C with a room temperature lattice parameter of 0.4228 nm would contain ca. 25 at% Co. It is an open question whether the protoxide in this sample would become the alleged equilibrium composition, i.e., 75 at% Co [15] by prolonged annealing at 850°C.

The M_1C_9 samples fired at 1600°C for 5 h (Fig. 2a) or subject to further annealing at 800°C for 72 h (Fig. 2b) contain additional spinel phase besides the protoxide. Least-squares fit of the d-spacings indicated the protoxide has a lattice parameter of 0.4257 ± 0.0001 nm and 0.4260 ± 0.0003 nm, respectively for the samples fired at 1600°C and 800°C. These lattice parameters are smaller than and equal to undoped $Co_{1-x}O$ (0.4260 nm, JCPDS#09-0402), respectively indicating a considerable dissolution of smaller-size Mg^{2+} in $Co_{1-x}O$ at 1600°C but negligible dissolution of Mg in $Co_{1-x}O$ at 800°C. The spinel oxide derived from $Co_{1-x}O$ component by oxidation upon rapid cooling from 1600°C (Fig. 2a) was too scarce to give adequate XRD peaks for precise lattice parameter determination. However, the spinel in the sample annealed at 800°C gave more significant peaks (Fig. 2b) for the determination of a room temperature lattice parameter 0.8083 nm. This cell parameter is slightly smaller than that undoped and cooled from 800°C (0.8086 nm) [8] in accord with Mg^{2+} doping as addressed later.

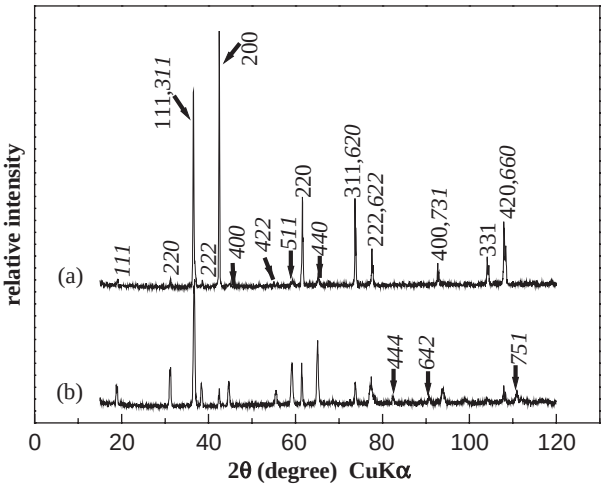

Fig. 2. XRD traces for M_1C_9 samples: (a) fired at 1600°C for 5 h and (b) subject to further annealing at 800°C for 72 h and then air-quenched. The diffractions of the protoxide and spinel phase are denoted by h k l and italic *h k l*, respectively.

SEM observations indicated the protoxide grains are smaller in size for M_9C_1 than M_1C_9 sample when sintered at 1600°C for 5 h (Figs. 3a and b). Intragranular faceted pores were only found in M_1C_9 sample upon thermal etching at 1500°C (Fig. 3b). Further annealing at 850°C for M_9C_1 sample and 800°C for M_1C_9 sample did not cause appreciable change of the grain size (not shown).

3.2. AEM

3.2.1. M_9C_1 sample

The M_9C_1 sample fired at 1600°C for 5 h and then air quenched showed dislocations predominantly aligned along ⟨110⟩ directions (Fig. 4a) and free of defect clusters even at grain boundaries (Fig. 4b). Further annealing at 850°C for 96 h caused planar defect modulation parallel to $(3\bar{1}1)$ for the protoxide as shown in the bright field image (Fig. 5a). The corresponding SAED pattern showed no side-band spots around the fundamental rock salt diffractions. Dark field image further showed complicated diffraction contrast in rock salt type matrix (Fig. 5b) presumably domains yet to be determined for their nature. These domains may be irregular point defect clusters as a result of 10 at% dissolution of cobalt in MgO according to point-count EDX analysis (Fig. 5c).

3.2.2. M_1C_9 sample

The M_1C_9 sample sintered at 1600°C for 5 h and then air quenched showed that the {111}-faceted spinel was precipitated within the protoxide grain (Fig. 6a). SAED pattern taken from the protoxide and the spinel indicated the two phases followed parallel epitaxial relationship. The spinel contains paracrystalline distribution of defect clusters as indicated by side-band diffraction spots in the inset SAED pattern in Fig. 6a. Lattice image (not shown) indicated that dislocations/faults are negligible for the spinel precipitate formed in such a rapid cooling process. The spinel precipitates were commonly dragged by tangled dislocations in the matrix, which gave diffuse diffraction intensity, but not clear side-band spots around the fundamental rock salt diffractions (Fig. 6b). Point count EDX analysis indicated the spinel (Fig. 6c) has a much lower Mg content than the protoxide (Fig. 6d).

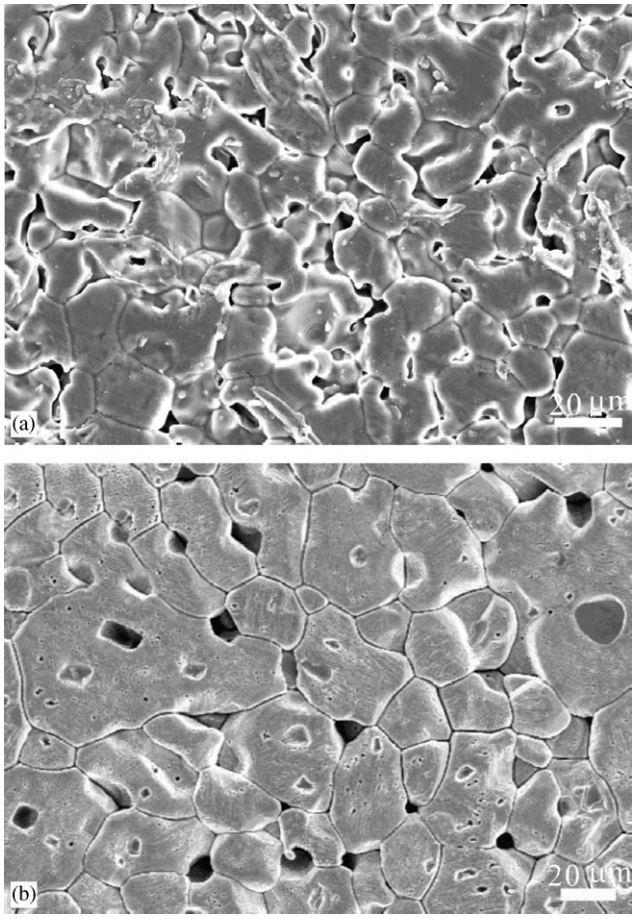

Fig. 3. SEM image (secondary electron image) of (a) M_9C_1 and (b) M_1C_9 sample prepared by sintering at 1600°C for 5 h and then thermally etched at 1500°C for 10 min. Note much larger grains with intragranular faceted pores in M_1C_9 sample.

Further annealing at 800°C for 72 h caused dislocation tangle and impingement of the coarsened spinel precipitates (Fig. 7a). The spinel in fact contained paracrystalline state of defect clusters as indicated by the side-band diffraction spots in [111] zone axis. Fig. 7b showed in further details the impinged spinel precipitates in the protoxide grain in [011] zone axis. The spinel paracrystal diffractions were clearly observed in the SAED pattern in Fig. 7c. The paracrystal {111} *d*-spacing of Mg-doped $Co_{3-\delta}O_4$ can be determined unambiguously to be 9 times the spinel {111} *d*-spacing

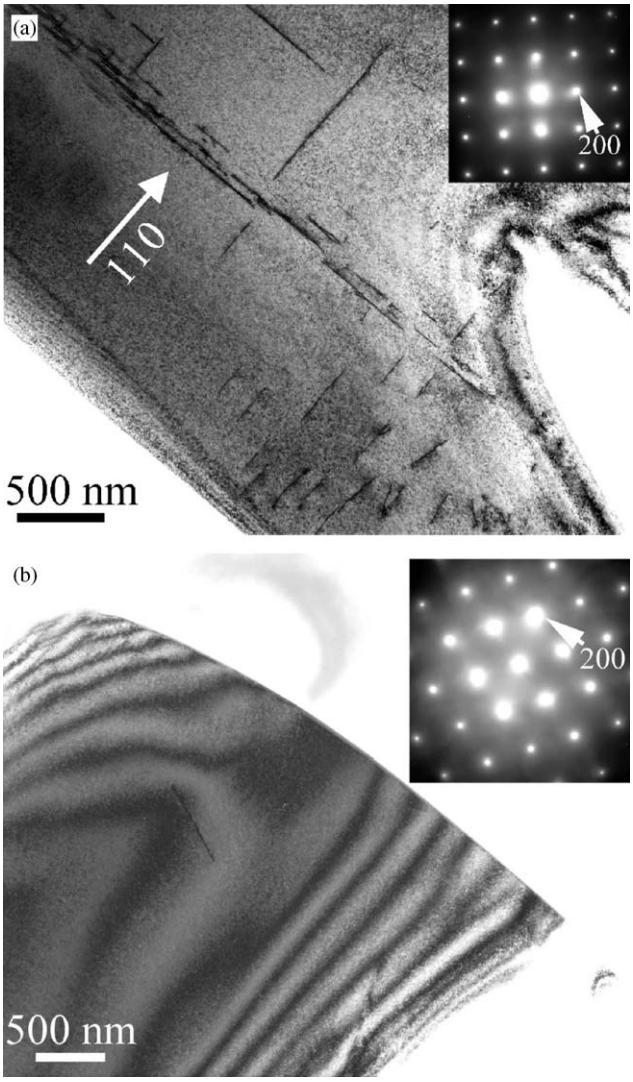

Fig. 4. TEM (a) bright field image (BFI) with inset SAED pattern in [001] zone axis showing dislocations predominantly aligned along ⟨110⟩ directions. (b) BFI with inset SAED pattern in [011] zone axis showing grain boundary free of defect clusters. The M_9C_1 sample fired at 1600°C for 5 h and then air quenched.

(4.22 nm) based on the side-band diffraction spots (Figs. 6a and 7c). This paracrystalline spacing is about 4.5 times that of the average spinel cell dimension. The side-band diffraction spots around the spinel {220} diffractions or their multiples in [001] zone axis, analogous to those shown in Fig. 3a of Ref. [8] for undoped $Co_{3-\delta}O_4$ paracrystal, gives the same paracrystalline spacing. Lattice image, taken from the coarsened/impinged spinel, showed (*hkl*)-specific coherency across the (111) interface of rock salt and spinel structure (Fig. 8a). The reconstructed image from the interface in fact showed coherent (200) plane across the interface, yet dislocations/fault parallel to (111) for both the protoxide and spinel (Fig. 8b). Away from the interface, there were still such dislocations and faults (Fig. 8c). It is noteworthy that lattice image showed a clear paracrystal array for

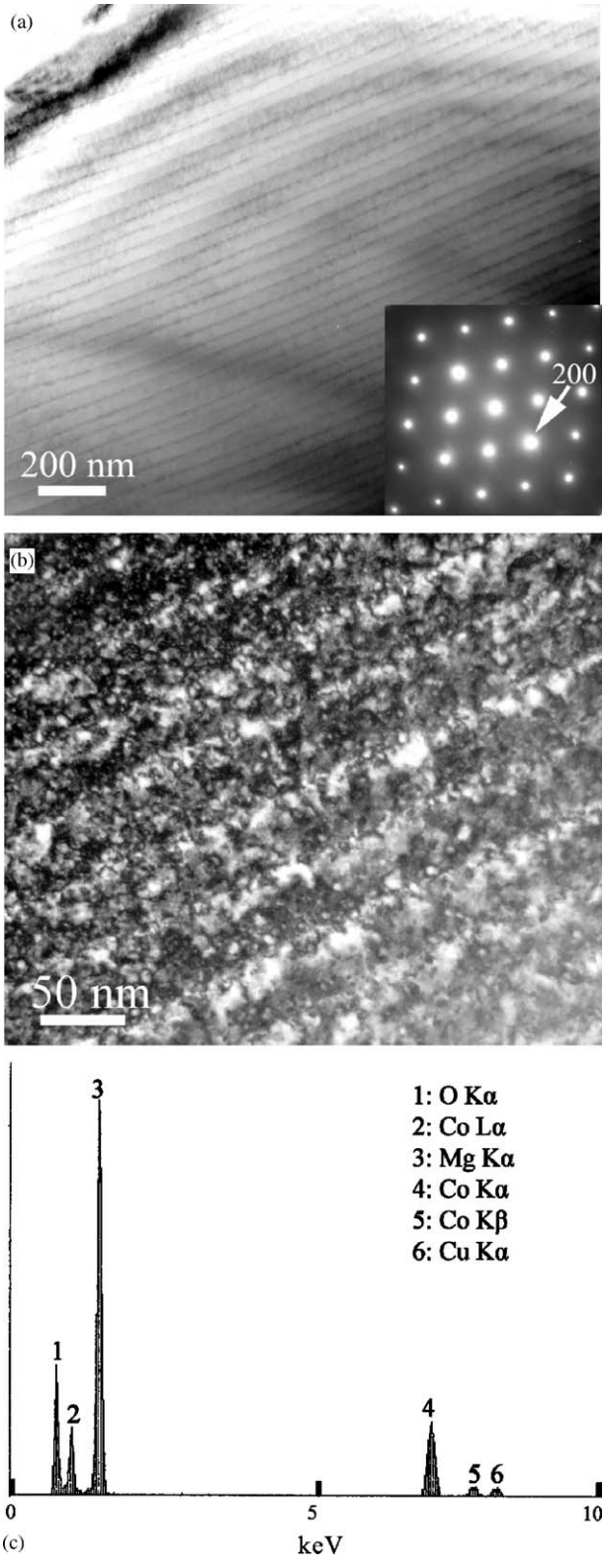

Fig. 5. TEM (a) BFI with inset SAED pattern of Co-dissolved MgO in [011] zone axis showing $(3\bar{1}1)$ planar modulation and absence of paracrystal diffraction spots. (b) Dark field image ($g = 200$) showing complicated diffraction contrast associated with $(3\bar{1}1)$ planar defect modulation. (c) Point-count EDX spectrum of the protoxide. M_9C_1 samples fired at 1600°C for 5 h and then further annealed at 850°C for 96 h followed by air-quenching.

undoped $Co_{3-\delta}O_4$ paracrystal [8], but a rather inhomogeneous paracrystal array for the present Mg-doped $Co_{3-\delta}O_4$ analogous to $Fe_{1-x}O$ [2]. Imaging such defect clusters by side-band spots is difficult, if not impossible, due to the interference of nearby spinel diffraction spots.

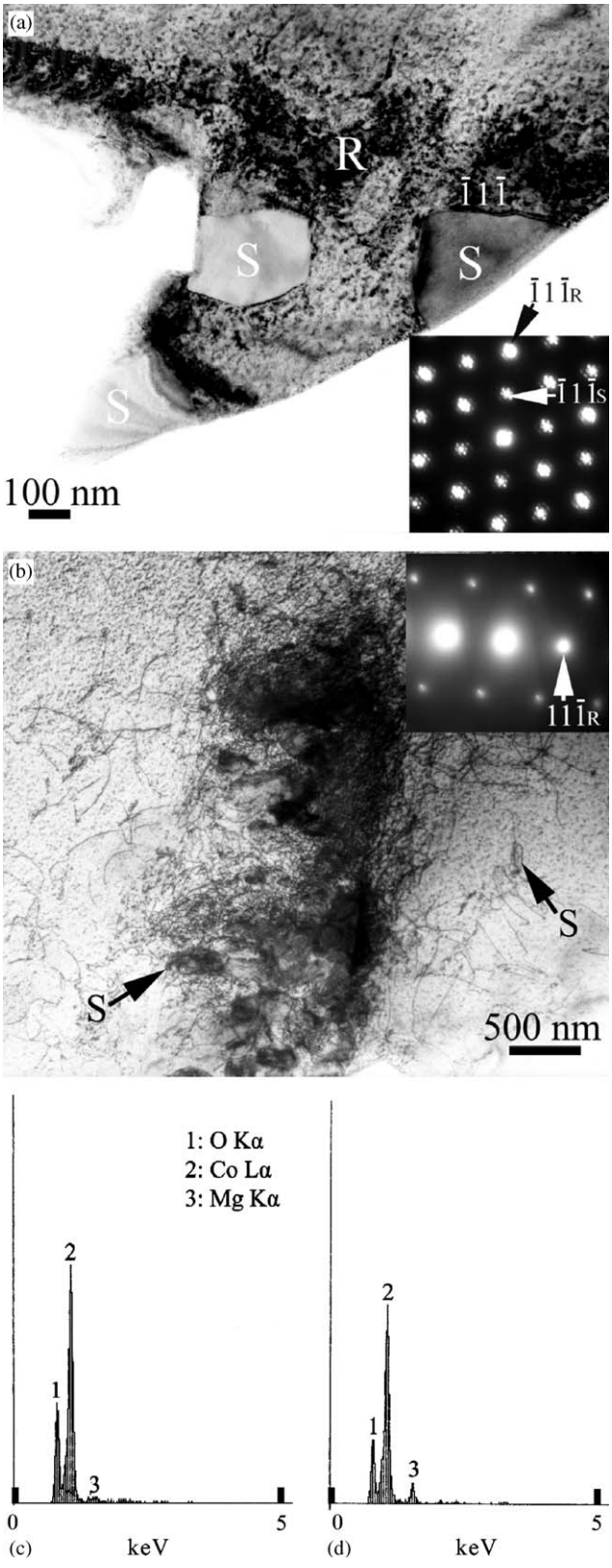

Fig. 6. TEM (a) BFI of {111}-faceted spinel (denoted as S) precipitated from Mg-dissolved $Co_{1-x}O$ with rock salt structure (denoted as R). The inset SAED pattern in [011] zone axis shows diffraction spots of R and S phases in parallel epitaxy and side-band spots of the paracrystal. (b) BFI of another Mg-dissolved $Co_{1-x}O$ grain with {111}-faceted and Mg-doped $Co_{3-\delta}O_4$ spinel nucleated at tangled dislocations (arrows). The inset SAED pattern (in [011] zone axis, not to scale of that in (a)) shows diffuse diffraction intensity around the diffraction spots of rock salt structure. (c) and (d) point count EDX spectrum of Mg-doped $Co_{3-\delta}O_4$ spinel and more Mg-dissolved $Co_{1-x}O$, respectively. M_1C_9 sample prepared by sintering at 1600°C for 5 h and then air quenched.

4. Discussion

4.1. Defect chemistry

Temperature-dependent P_{O_2} in atmosphere accounts for the oxidation of undoped $Co_{1-x}O$ to form $Co_{3-\delta}O_4$ spinel below 900°C [10]. In such an oxidation process, cobalt vacancies (V''_{Co}), interstitials $(Co_i^{\cdots})$, and 4:1 clusters $([Co_i^{\cdots} + 4V''_{Co} + 4Co^{\bullet}_{Co}])$ were assembled as paracrystal for $Co_{1-x}O$ and even $Co_{3-\delta}O_4$ spinel [8]. In the present MgO–$Co_{1-x}O$ system, Mg dopant is also of concern on the defect clustering in $Co_{1-x}O$ and paracrystal formation in $Co_{3-\delta}O_4$ as addressed in turn.

4.1.1. Mg-doped $Co_{1-x}O$

A smaller X-ray lattice parameter for Mg-doped $Co_{1-x}O$ (0.4257 nm) than undoped $Co_{1-x}O$ (0.4260 nm) indicated that Mg^{2+} (effective ionic radii, 0.0720 nm) replaced Co^{2+} in high spin (0.0745 nm) rather than low spin state (0.0650 nm) in CN 6 [17]. The undersized dopant Mg^{2+} in the Co^{2+} site could also force further cobalt ion to enter the interstitial site as $Co_i^{\cdots}$, which then induced charge-compensating cation vacancies and 4:1 defect clusters through the following equation in Kröger–Vink notation [18]:

$$MgO \xrightarrow{CoO} Mg^{x}_{Co} + [Co_i^{\cdots} + 4V^{\bullet}_{C_o} + 5h^{\bullet}] + O^{x}_{O}. \quad (1)$$

Here Mg^{x}_{Co} signifies a noncharged magnesium at cobalt sites in the crystal lattice and $h^{\bullet}$ could be associated with V''_{Co} to form V'_{Co} or associated with Mg^{x}_{Co} to form $Mg^{\bullet}_{Co}$. The resultant 4:1 type defect clusters can then be activated to form paracrystalline ordered state and then spinel.

The {111} faulting of Mg-dissolved $Co_{1-x}O$ near the interface of rock salt and spinel structure may imply the assembly of excess vacancies along close-packed {111} planes vulnerable to crystallographic shear. It is of interest to note that such fault also occurred for $Co_{1-x}O$ near the Kirkendall pores upon interdiffusion with yttria-partially stabilized zirconia [19].

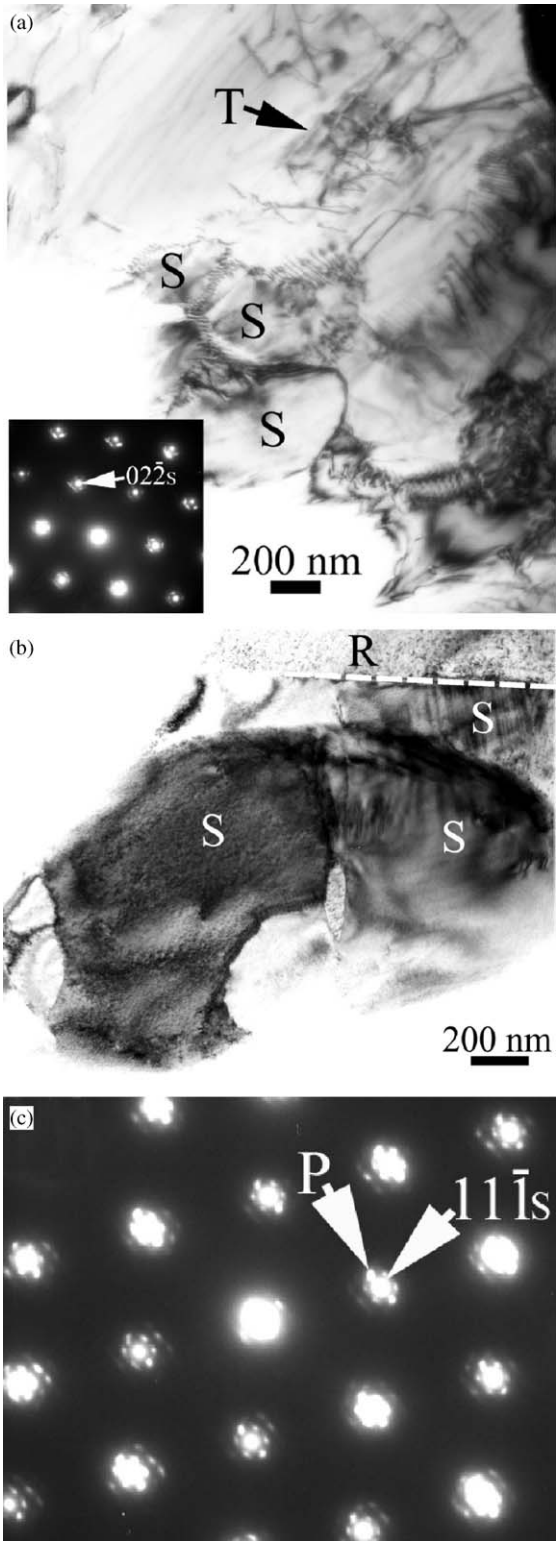

Fig. 7. TEM (a) BFI showing impinged spinel (denoted as S) precipitates and dislocation tangle (denoted as T) upon annealing. The inset SAED pattern in [111] zone axis shows side-band diffractions of paracrystal around spinel diffractions. (b) BFI of impinged spinel precipitates in protoxide matrix of rock salt structure (denoted as R). (c) SAED pattern of spinel precipitate in [011] zone axis showing side band spots of paracrystal (denoted as P). M_1C_9 sample sintered at 1600°C and then annealed at 800°C for 72 h followed by quenching in air.

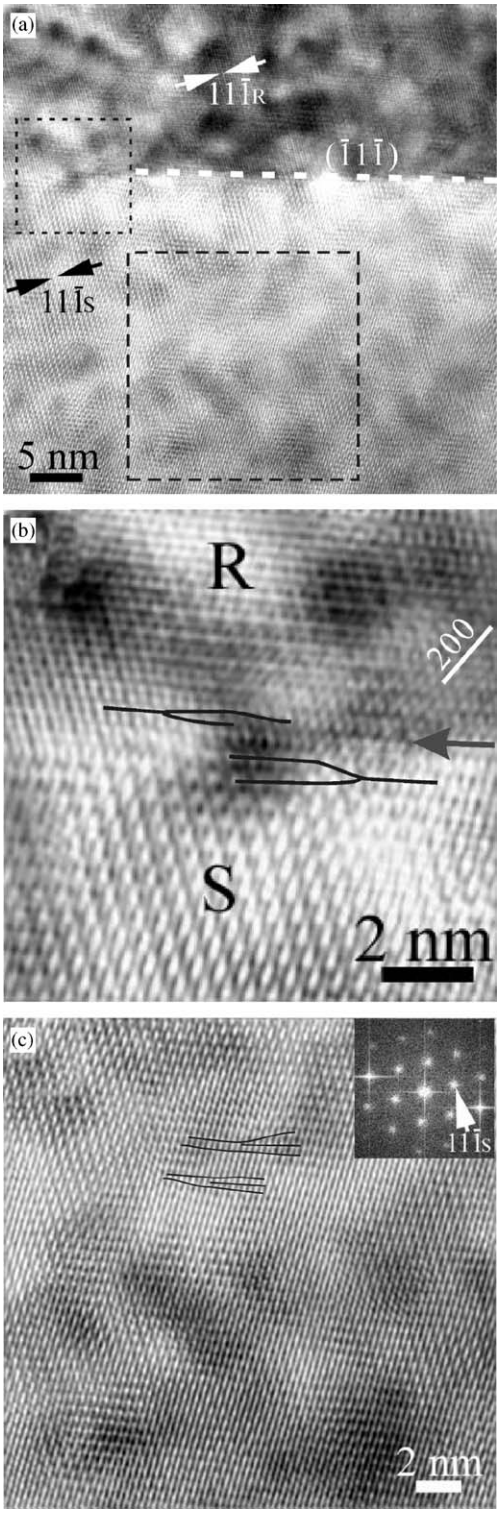

Fig. 8. (a) Lattice image taken from the (111) R/S interface denoted by dashed line in Fig. 7b. (b) Reconstructed image (inverse Fourier transform) from the small squared region in (a) showing dislocations/fault (as delineated by solid lines) parallel to (111) for both the protoxide and spinel phases near the R/S interface (arrow). (c) Reconstructed image and 2-D Fourier transform (inset) from the large squared region in (a) showing the spinel precipitate is full of dislocations/fault parallel to (111) as delineated by solid lines. The same specimen as Fig. 7.

4.1.2. Mg-doped $Co_{3-\delta}O_4$

The defect structure of normal $Co_{3-\delta}O_4$, which can be described by the formula $(Co^{2+}_{tet})_8(Co^{3+}_{oct})_{16}(V_{oct})_{16}(O^{-2})_{32}$, is not well known but cation vacancies seem to be predominant lattice defects in this structure [20]. The paracrystal of undoped $Co_{3-\delta}O_4$ may be assembled from cobalt vacancies and cobalt interstitials via defect equations analogous to the case of parent $Co_{1-x}O$ [8]. The extra Co^{3+} deviating from stoichiometric spinel, as denoted by δ in the formula $Co_{3-\delta}O_4$, may occupy both tetrahedral A sites and octahedral B sites at high temperatures as the case of so-called disordered spinel above 1150 K [21]. As for Mg-doped $Co_{3-\delta}O_4$, its δ value was raised by Mg-dopant (see Section 4.3.). The extra cobalt vacancies and Co^{3+} interstitials in Mg-doped $Co_{3-\delta}O_4$ may form extra 4:1 defect clusters analogous to Eq. (1) for parent Mg-dissolved $Co_{1-x}O$. In the framework of alternating $Co^{2+}O_4$ tetrahedra and $Co^{3+}_4O_4$ cubes, which build up into a face centered cubic lattice of 32 oxygen ions [20], these extra 4:1 defect clusters may more or less link to affect the paracrystal spacing for $Co_{3-\delta}O_4$.

The {111} faulting of Mg-doped $Co_{3-\delta}O_4$ spinel, analogous to that of the (Zr,Y)-codoped $Co_{3-\delta}O_4$ spinel [22], may be a result of specific arrangement of Co vacancies within the spinel framework and its monoxide precursor. Our tentative explanation is that the (111) faulting implies the presence of zinc blende type defect clusters (e.g. 16:7 derived from 4:1 clusters by corner sharing [23]) in Mg-dissolved $Co_{1-x}O$ and Mg-doped $Co_{3-\delta}O_4$, because such types of cluster have cation vacancies assembled along oxygen close-packed (111) plane, which is beneficial for crystallographic shear. This mechanism may be valid for specific temperature-time path because such fault occurred in both rock salt and spinel structures when annealed at 800°C (Fig. 8) but not upon rapid cooling from 1600°C.

4.1.3. Co-doped MgO

The Co-doped MgO did not form appreciable paracrystal distribution of defect clusters or spinel precipitates regardless of prolonged annealing in the stability field of $Co_{3-\delta}O_4$ spinel, i.e., at 850°C in air. This indicates that the substitution of isovalent but oversized Co^{2+} for Mg^{2+} in octahedral sites and resultant Co^{3+} in tetrahedral interstitial sites generate only a limited number of volume- and charge-compensating defects through the following equation:

$$CoO\underline{^{MgO}}Co^{x}_{Mg} + [V''_{Co} + Co^{\bullet}_{Co}] + h^{\bullet} + O^{x}_{O}. \quad (2)$$

Here Co^{x}_{Mg} signifies a noncharged cobalt at magnesium sites in the crystal lattice. It is also possible that the volume compensating effect due to the substitution of larger Co^{2+} with Mg^{2+} in CN 6 [17] forced $Co^{\bullet}_{Co}$ to enter the interstitial tetrahedral site, i.e., $Co^{\cdots}_{Co}$, and hence more charge-compensating cation vacancies through the following equation:

$$Co^{x}_{Mg} + [V''_{Co} + Co^{\bullet}_{Co}] - Co^{x}_{Mg} + [Co^{\cdots}_{i} + 4V''_{Co} + 4Co^{\bullet}_{Co}]. \quad (3)$$

It should be noted that more cobalt ion may become high spin state in CN 6 and/or entered the interstitial site so that the Co-dissolved MgO has a larger lattice parameter 0.4228 nm when annealed at 850°C, in comparison with 0.4223 nm for the sample quenched from 1600°C. In any case, the 4:1 type defect clusters formed through Eqs. (2) and (3) are probably isolated or screened by a rather refractory MgO matrix to prevent from further linkage into paracrystalline distribution of defect clusters or spinel phase. The $(3\bar{1}1)$ planar modulation appeared to be an alternative means for defect relaxation upon prolonged annealing at 850°C (Fig. 5a). Such modulation may be due to specific soft mode dynamics and/or spinodal-like composition variation yet to be clarified.

4.2. Heterogeneous nucleation of defect clusters and spinel

Paracrystal is expected to nucleate at free surface and dislocations where intrinsic/extrinsic defects segregate and short-circuit diffusion prevails. The work function measurements of the cleaved $Co_{1-x}O$ single crystal indeed showed that intrinsic defects preferred to occur at free surface and therefore the Co_3O_4 structure formed within the near-surface layer under TP_{O_2} conditions, which correspond to the stability of the CoO phase in the bulk [20]. It is an open question whether the phase diagram dealing with near-surface or near-interface consecutive regimes of forming cobalt vacancies and then cobalt interstitials from $Co_{1-x}O$ can be extended to the case of generating such defects from $Co_{3-\delta}O_4$, either undoped [8] or Mg-doped. If near-surface or near-interface consecutive regimes are indeed effective for Mg-doped $Co_{3-\delta}O_4$, then the paracrystals are expected to form above 900°C, the equilibrium $Co_{1-x}O/Co_{3-\delta}O_4$ phase boundary for the bulk in air [10].

Dislocations, generated by sintering/coalescence process as demonstrated by the assembly of nanocrystalline titania [24] and CeO_2 [25], may also act as nucleation sites of the paracrystal. The space charge at these sites, as expected for rock salt-type ionic crystals [26], may favor clustering of charged species into the 4:1 and then paracrystalline ordered state.

4.3. Implications of spacing between defect clusters

The spacing of defect clusters is 4.5 times the lattice spacing of the average spinel structure of Mg-doped $Co_{3-\delta}O_4$. This spacing between defect clusters is about 0.9 times that of our previously studied case of undoped

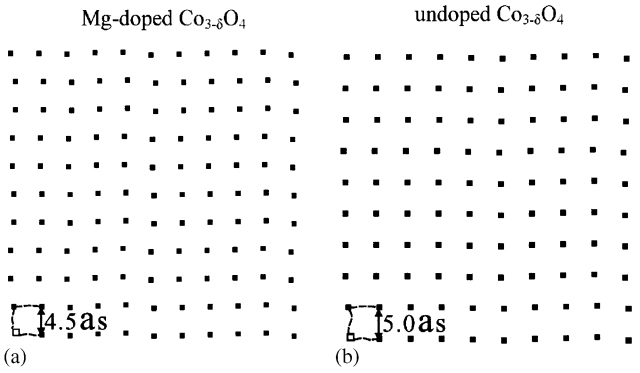

Fig. 9. Schematic drawing ([100] projection in real space) of the paracrystalline distribution of 4:1-type-derived defect clusters (solid squares) with nearly 4.5 and 5 times the lattice spacing of the average structure for (a) Mg-doped $Co_{3-\delta}O_4$, and (b) undoped $Co_{3-\delta}O_4$ (after ref. [8]), respectively. The unit cell (small square) dimension of spinel type structure is denoted as **as**.

$Co_{3-\delta}O_4$ [8] as depicted schematically in Fig. 9. In other word, there is about 0.73 (i.e., $0.9 \times 0.9 \times 0.9$) times difference in defect-cluster concentration if defect clusters are of the same type in the two lattices and the effect of defect clustering on electronic configuration and interionic distance is negligibly low [27]. The δ value of Mg-doped $Co_{3-\delta}O_4$ is thus ca. 1.37 (i.e. 1/0.73) times higher than undoped $Co_{3-\delta}O_4$. This indicates that isovalent yet size-mismatched Mg^{2+} is an effective dopant for the generation of volume- and hence charge-compensating defects in the $Co_{3-\delta}O_4$ spinel. The parent rock salt structure, however, hardly showed paracrystals. This can be explained by complete exsolution of Mg^{2+} from $Co_{1-x}O$ to form Mg-doped $Co_{3-\delta}O_4$ at 800°C according to X-ray lattice parameter of rock salt structure mentioned above. As for industrial implication, dopant-tailored spinel paracrystal is expected to affect catalytically active surface/bulk of cobalt oxide catalysts and may have potential applications as step-wise sensor of oxygen partial pressure at high temperatures.

5. Conclusions

1. The protoxide of Co-doped MgO decomposed to form planar defect modulation when annealed at 850°C in air.
2. The protoxide of Mg-doped $Co_{1-x}O$ exsolved to form spinel paracrystal when cooled from 1600°C or annealed at 800°C in air.
3. Paracrystalline ordered state can hardly be identified for Mg-doped $Co_{1-x}O$ due to a rather rapid consumption of defect clusters to form spinel phase upon exsolution.
4. The Mg-dopant introduced extra cobalt vacancies and Co^{3+} interstitials for $Co_{3-\delta}O_4$ to form a smaller interspacing of paracrystal, i.e., 4.5 instead of 5.0 times that of average spinel lattice parameter. The δ value of Mg-doped $Co_{3-\delta}O_4$ is calculated to be ca. 1.37 times higher than undoped $Co_{3-\delta}O_4$.
5. The {111} faulting of Mg-doped $Co_{3-\delta}O_4/Co_{1-x}O$ implies the possible presence of zinc blend-type defect clusters with cation vacancies assembled along oxygen close packed (111) plane.

Acknowledgments

This research was supported by National Science Council Taiwan, ROC and Center for Nanoscience and Nanotechnology at NSYSU. We thank an anonymous referee for valuable comments.

References

[1] T.R. Welberry, A.G. Christy, J. Solid State Chem. 117 (1995) 398–406.
[2] T.R. Welberry, A.G. Christy, Phys. Chem. Mineral. 24 (1997) 24–38.
[3] B.E.F. Fender, F.D. Riley, in: Non-Metallic Solids, L. Eyring, M. O'Keefe (Eds.), The Chemistry of Extended Defects, North-Holland, Amsterdam, 1970.
[4] C.R.A. Catlow, B.E.F. Fender, J. Phys. C: Solid State Phys. 8 (1975) 3267–3279.
[5] P. Vallet, P. Raccah, Mem. Sci. Rev. Metall. 62 (1965) 1–29.
[6] B. Andersson, J.O. Sletnes, Acta Crystallogr. Sect. A 33 (1977) 268–276.
[7] S.M. Tomlinson, C.R.A. Catlow, J.H. Harding, J. Phys. Chem. Solids 51 (1990) 477–506.
[8] W.H. Lee, P. Shen, J. Solid State Chem. 177 (2004) 101–108.
[9] P. Cossee, Rec. Trav. Chim. Pays-Bas 75 (1956) 1089–1096.
[10] M. Oku, Y. Sato, Appl. Surf. Sci. 55 (1992) 37–41.
[11] J.A. Duffy, Bonding, Energy Levels and Bands in Inorganic Solids, Longman Science Technology, Essex, 1990, p. 137.
[12] W.H. Strehlow, E.L. Cook, J. Phys. Chem. Ref. Data 2 (1973) 163–200.
[13] H.L. Tuller, Mixed Conduction in Nonstoichiometric Oxides, in: O.T. Sørensen (Ed.), Nonstoichiometric Oxides, Academic Press, New York, 1981, p. 302.
[14] Y. Moriyoshi, T. Ikegami, Dislocations in MgO, in: W.D. Kingery (Ed.), Advances in Ceramics, Vol. 10, Structure and properties of MgO and Al_2O_3 Ceramics, The American Ceramic Society, Columbus, OH, 1984, pp. 258–274.
[15] E.M. Levin, C.R. Robbins, H.F. McMurdie, Phase Diagram for Ceramists, compiled at the Nation Bureau of Standards, edited and published by The American Ceramic Society, Inc., 1964, Fig. 51, p. 51.
[16] D.B. Williams, Practical Analytical Electron Microscopy in Materials Science, Philips Electronic Instruments, Inc., Electron Optics Publishing Group, Mahwah, NJ, 1984, p. 157.
[17] R.D. Shannon, Acta Crystallogr. Sect. A 32 (1976) 751–767.
[18] F.A. Kröger, H.J. Vink, Solid State Phys. 3 (1956) 307–435.
[19] W.H. Lee, P. Shen, Micron 33 (2002) 555–559.
[20] J. Nowotny, W. Weppner, M. Sloma, Near-surface defect structure of CoO in the vicinity of the CoO/Co_3O_4 phase boundary, in: J. Nowotny, W. Weppner (Eds.), Non-Stoichiometric Compounds Surfaces, Grain Boundaries and Structural

Defects, Kluwer Academic Publishers, Dordrecht, 1989, pp. 265–277.
[21] X. Liu, C.T. Prewitt, Phys. Chem. Mineral. 17 (1990) 168–172.
[22] K.T. Lin, P. Shen, J. Solid State Chem. 145 (1999) 739–750.
[23] A.B. Anderson, R.W. Grimes, A.H. Heuer, J. Solid State Chem. 55 (1984) 353–361.
[24] R.L. Penn, J.F. Banfield, Science 281 (1998) 969–971.
[25] W.H. Lee, P. Shen, J. Crystal Growth 205 (1999) 169–176.
[26] A. Atkinson, R.I. Taylor, Philos. Mag. A 43 (1981) 979–998.
[27] W.L. Smith, A.D. Hobson, Acta Crystallogr. B 29 (1973) 362–363.